

# Joint Source-Environment Adaptation of Data-Driven Underwater Acoustic Source Ranging Based on Model Uncertainty

Dariush Kari, Hari Vishnu, *Senior Member, IEEE*, Andrew C. Singer, *Fellow, IEEE*

**Abstract**—Adapting pre-trained deep learning models to new and unknown environments is a difficult challenge in underwater acoustic localization. We show that although pre-trained models have performance that suffers from mismatch between the training and test data, they generally exhibit a higher “implied uncertainty” in environments where there is more mismatch. Leveraging this notion of implied uncertainty, we partition the test samples into more certain and less certain sets, and implement an estimation method using the certain samples to improve the labeling for uncertain samples, which helps to adapt the model. We use an efficient method to quantify model prediction uncertainty, and an innovative approach to adapt a pre-trained model to unseen underwater environments at test time. This eliminates the need for labeled data from the target environment or the original training data. This adaptation is enhanced by integrating an independent estimate based on the received signal energy. We validate the approach extensively using real experimental data, as well as synthetic data consisting of model-generated signals with real ocean noise. The results demonstrate significant improvements in model prediction accuracy, underscoring the potential of the method to enhance underwater acoustic localization in diverse, noisy, and unknown environments.

**Index Terms**—underwater acoustics, localization, domain adaptation, source hypothesis transfer, mismatch

## I. INTRODUCTION

DEEP learning (DL)-based underwater acoustic (UWA) localization algorithms [1]–[4] tend to generalize poorly to mismatched environments [3], [5], [6]. To overcome small mismatches between the testing and training sets, domain adaptation (DA) methods match some of the statistics of the testing data to those of the training data [7], which, at inference time, requires access to the training data acquired with known or controlled sources. However, for low-power underwater devices working in a decentralized manner [8]–[10], training data will not always be available at the inference device, either due to the communication cost of transferring large

datasets between such devices, or security or privacy issues. Therefore, this paper seeks to improve the generalization performance of DL-based models for UWA localization via *test-time adaptation* (TTA)<sup>1</sup> [11].

To provide a more robust solution than matched field processing (MFP) [12], [13], Chen and Schmidt [3] propose a model-based convolutional neural network (CNN) that outperforms MFP in the presence of sea depth mismatch. It generates the training data using a propagation model with the sound speed profile (SSP) set according to the values measured in a real experiment. This method ignores the parameter shift between the synthetic training data and the real testing data and assumes accurate prior knowledge of the parameters of the test environment, which is rarely available. This motivates further improvement using an adaptation mechanism.

The environmental mismatch problem is known in the machine learning literature as domain shift [14], and has been tackled with approaches including domain adaptation or generalization [11], [14], meta learning [15], transfer learning [16], [17], and data augmentation [18]. Transfer learning requires labels for some of the test data, which are usually not available in UWA problems and encourages pursuit of DA methods. Moreover, although DA and transfer learning have been studied for some cases in underwater acoustic localization [16], [19], [5], [20], more extensive investigations into DA are warranted.

Domain adaptation can leverage training data whenever available to learn any underlying domain shift. For UWA localization, inspired by deep subdomain adaptation networks [21], Liu, et al. [5] propose an unsupervised DA method that aims to align the feature distributions of training and test data at every layer of the network. Long, et al. [20] apply an adversarial method based on [7] to extract useful features that are invariant with respect to domain shifts. This approach adds a domain classifier to the original deep model and uses a training loss designed to promote features that confuse this domain classifier in order to achieve domain invariance. These methods, though effective, rely on access to training data. In the absence of training data, TTA is still possible by inferring some useful statistics (features) of the training set from the pre-trained model itself [11].

<sup>1</sup>Note that in machine learning parlance, test-time adaptation is also called source-free adaptation, where “source” refers to the training domain. However, to avoid confusion with the acoustic source, we use the term test-time adaptation.

This work has been supported by the Office of Naval Research (ONR) under grant N00014-19-1-2662.

Manuscript received August 1, 2024; revised September 16, 2024. (Corresponding author: Dariush Kari)

Dariush Kari is with the Interdisciplinary Health Sciences Institute (IHSI), University of Illinois Urbana-Champaign, Urbana, IL 61801, USA (email: dkari2@illinois.edu).

Hari Vishnu is with Acoustic Research Laboratory, National University of Singapore, Tropical Marine Science Institute, Singapore 119222 (email: harivishnu@gmail.com)

Andrew C. Singer is with the Department of Electrical and Computer Engineering, Stony Brook University, Stony Brook, NY 11794, USA (email: andrew.c.singer@stonybrook.edu).

There is a rich literature on TTA including source hypothesis transfer (SHOT) [11], entropy minimization [22], universal TTA [23], contrastive TTA [24], adaptive adversarial network-based TTA [25], and distribution estimation [26]. To perform TTA, we leverage an implied model uncertainty [27]–[30]. Although conformal prediction [31] has recently been adopted for uncertainty quantification in data-driven UWA localization [32], it requires a labeled dataset from the test environment for calibration. To explore the effects of mismatch on model uncertainty without any labeled dataset available at the test time, we adopt model uncertainty using mutual information (MUMI) [29]. To avoid the computational burden of MUMI during adaptation, in Section III-B, we cast the ranging problem as a classification task that can leverage computationally simpler *implied* uncertainty quantification methods such as peakwise uncertainty (PU). Our observations in Section III demonstrate that both MUMI and PU increase with an increase in the amount of mismatch.

Environmental mismatches do not affect all samples to the same extent - some samples are affected more and result in a higher uncertainty. For instance, the signal received by the receiver array from a source at a short distance is dominated by the direct path arrivals and first-order reflected raypaths (single reflection from either surface or bottom) [33]. Thus, the depth mismatch affects farther sources more significantly due to the contribution of higher-order bottom reflections received by the array. We study source ranging problems in which there are diverse test samples from different ranges associated with the same source. By partitioning the test samples into certain and uncertain sets based on their PU scores, we can implicitly infer the source power.

Typical data-driven methods in UWA signal processing perform normalization with respect to the received signal strength to obtain source-invariant features [1]. However, this discounts the information in the received signal strength which can aid UWA localization, as demonstrated by some methods [34], [35]. A pre-trained network deprived of the source power information, as discussed in Section III-B, will be confused in the presence of environmental mismatches. To reduce the model confusion, we develop another robust and coarse estimation process based on the received signal strength named the joint source-environment adaptation (JSEA). This leverages the set of certain test samples and enhances the generalization across different environments, while retaining the source-invariance property of the pre-trained model.

The rest of the paper is organized as follows. Section II provides the necessary background on the MFP and CNN approaches for localization. Section III investigates uncertainty quantification in the UWA localization problem. Section IV provides the SHOT approach to adaptation and our proposed method for JSEA. Finally, Section V demonstrates the efficacy of the proposed method on several synthetic and real datasets, followed by some concluding remarks in Section VI.

## II. LOCALIZATION USING SAMPLE COVARIANCE MATRICES

**Notation:** Bold letters denote matrices and vectors,  $H(\mathbf{y})$  indicates the discrete entropy of a probability mass function

(PMF)  $\mathbf{y}$ ,  $D_{KL}$  denotes the KL-divergence,  $\text{Re}(x)$  and  $\text{Im}(x)$  respectively denote the real and imaginary parts of  $x$ ,  $\mathbf{A}^T$  and  $\mathbf{A}^H$  denote respectively the transpose and conjugate transpose of the matrix or vector  $\mathbf{A}$ . For a set of test points  $\mathcal{S}$ , the complement is shown by  $\mathcal{S}^c = \mathcal{D}_{test} - \mathcal{S}$  and the cardinality is shown by  $|\mathcal{S}|$ .

Sample covariance matrices (SCM) are usually used for UWA array-based localization because they are sufficient statistics for the jointly Gaussian signal and noise [36] scenarios. The normalized SCM of an  $L$ -element array at a frequency  $f$  using  $P$  snapshots  $\tilde{\mathbf{r}}^{(p)}(f)$  is calculated as

$$\tilde{\mathbf{C}}(f) = \frac{1}{P} \sum_{p=1}^P \tilde{\mathbf{r}}^{(p)}(f) \tilde{\mathbf{r}}^{(p)}(f)^H, \quad (1)$$

where  $\tilde{\mathbf{r}}^{(p)}(f) = [\tilde{r}_1^{(p)}(f), \tilde{r}_2^{(p)}(f), \dots, \tilde{r}_L^{(p)}(f)]^T$  and

$$\tilde{r}_l^{(p)}(f) = \frac{r_l^{(p)}(f)}{\sqrt{\sum_{l=1}^L |r_l^{(p)}(f)|^2}}, \quad l \in \{1, 2, \dots, L\}, \quad (2)$$

where the scalar  $r_l^{(p)}(f)$  is the complex Fourier coefficient of the  $p$ -th segment of the received signal on the  $l$ -th hydrophone at the frequency  $f$ . For the synthetic data in the simulations, we use the KRAKEN-generated values for  $\tilde{r}_l^{(p)}(f)$ , while for the real data, we take the Fourier transform of the recorded temporal waveform, as explained in Section V-B.

### A. MFP approach

Given that the acoustic source propagates a narrowband signal at a frequency  $f$ , we use the Bartlett processor [37] as an MFP baseline, which is defined as

$$\hat{d} = \arg \max_d \tilde{\mathbf{r}}(f, d)^H \tilde{\mathbf{C}}(f) \tilde{\mathbf{r}}(f, d), \quad (3)$$

where  $\tilde{\mathbf{C}}$  is the normalized SCM of the measured data,  $\tilde{\mathbf{r}}(f, d)$  is the replica field at frequency  $f$  generated by a source at range  $d$ . For each  $d$ , the corresponding  $\tilde{\mathbf{r}}(f, d)$  (of the CNN approach) from the training set is used at inference time.

### B. CNN approach

Localization can be formulated as a regression or a classification problem [3], [38]. Classification models usually assume equidistant labels, as opposed to the regression models that preserve the distance among labels. To address this issue, rather than predicting the true class, we train the classification network to predict a softened label, viz. a PMF, based on the true class. This metric-inspired label softening preserves distances between different classes, makes the model more amenable to the localization problem, and facilitates the proposed uncertainty-based TTA approach. The proposed classification and regression models are both based on a CNN architecture, differing only in the last layer, as in [3].

The classifier CNN architecture is detailed as follows. As depicted in Fig. 1, the feature extractor part of the model consists of a CNN that takes the real and imaginary parts of the SCM,  $\mathbf{x}_i = [\text{Re}(\tilde{\mathbf{C}}_i), \text{Im}(\tilde{\mathbf{C}}_i)]$ , as a 2-channel input (a real tensor of dimension  $2 \times L \times L$ ) and a linear

layer that generates the feature vector  $\phi_i$ . These features are then fed into a linear classifier to generate the output PMF  $\hat{y}_i$ . Denoting the region of interest for the source range by  $[D_{\min}, D_{\max}]$ , for each training sample  $i$ , we quantize the range  $d_i$  by  $d_i^q = \lfloor \frac{d_i - D_{\min}}{B} + 0.5 \rfloor$  to obtain classification outputs with a resolution of  $B = 100$  m (and consequently, a PMF with bin size  $B = 100$  m). A one-hot representation of  $d_i^q$  is used in classification tasks. However, since we use mean absolute error (MAE) to evaluate our results, we define the soft label  $\mathbf{y}_i = [y_{i1}, y_{i2}, \dots, y_{iM}] = \eta(d_i^q)$  as

$$y_{ik} = \frac{\exp(-|k - d_i^q|/\sigma)}{\sum_{k=1}^M \exp(-|k - d_i^q|/\sigma)}, \quad (4)$$

where  $M$  is the number of classes and  $\sigma$  is a hyperparameter determining the spread of the peak in the soft label. A small  $\sigma$  effectively renders the labels one-hot coded while a large  $\sigma$  decreases the accuracy by encouraging high-entropy output labels. We empirically conclude that  $1 \leq \sigma \leq 10$  is appropriate for quantization bins of size  $B = 100$  m. Figure 2 shows an example of a soft label with  $\sigma = 5$ .

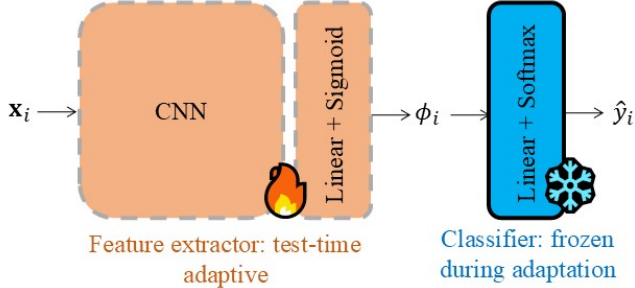


Fig. 1: The CNN classifier includes a feature extraction part followed by a linear classifier that will be frozen during adaptation.

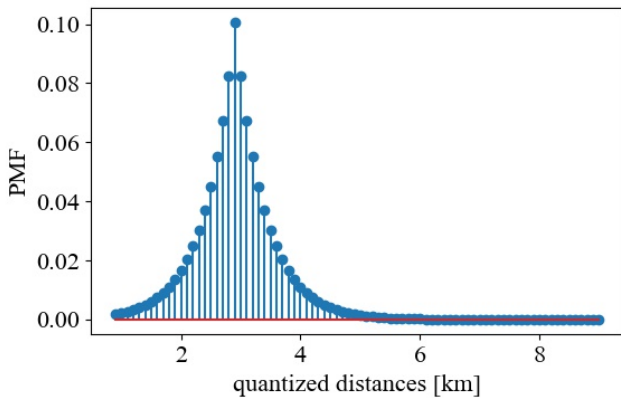


Fig. 2: An example of a metric-inspired smoothed label  $y_i$  corresponding to  $d_i = 2.9$  km or  $d_i^q = 20$ . Here, we have used the absolute error as the metric, hence, we have used a truncated exponential as the label. The quantization bins are 100 m wide.

Therefore, the training dataset is denoted by  $\mathcal{D}_{tr} = \{(\mathbf{x}_i, \mathbf{y}_i)\}_{i=1}^{N_{tr}}$  and the test set that does not include labels

is denoted by  $\mathcal{D}_{test} = \{\mathbf{x}_i\}_{i=1}^{N_{test}}$ . We use the loss function  $\mathcal{L}_{tr} = \frac{1}{N_{tr}} \sum_{i=1}^{N_{tr}} \text{CE}(\mathbf{y}_i, \hat{\mathbf{y}}_i)$  for training, where  $\hat{\mathbf{y}}_i$  is the network output and CE is the cross-entropy loss defined by

$$\text{CE}(\mathbf{y}_i, \hat{\mathbf{y}}_i) \triangleq - \sum_{k=1}^M y_{ik} \log \hat{y}_{ik}. \quad (5)$$

The CNN structure used herein is similar to that presented in [3] with a 2-channel input and 3 convolutional layers with 6, 38, and 40 channels and kernels of sizes 3, 5, and 5, respectively. The output of the feature extraction is a 256-dimensional vector  $\phi_i$ , which is then fed into the classifier to generate  $\hat{y}_i$ .

### III. MODEL UNCERTAINTY UNDER MISMATCH

For TTA, we first compute the uncertainty of the DL model about its estimations, and then implicitly extract the power of the acoustic source that generated the test data, from those test samples about which the model is most certain. We will discuss two uncertainty quantification methods that can be used with classification or regression models. Although localization naturally fits into a regression paradigm [38], regression models in their standard form only output point estimates. A stochastic regression model (e.g., a dropout network) can produce a PMF output by several realizations of the forward pass [29], which can then be used in MUMI or PU. However, the deterministic classification model already outputs a PMF in its forward pass, which can be used in the PU method.

#### A. Model Uncertainty using Mutual Information (MUMI)

There are two different sources of uncertainties in data-driven models [29], [30]: 1) epistemic that corresponds to the lack of training data and 2) aleatoric that corresponds to noisy or inherently ambiguous data. To alleviate the effects of mismatch between the training and test data, we focus on the epistemic uncertainty. Consider a dropout network with the weights vector  $\mathbf{w}$ . Treating  $\mathbf{w}$  as a random variable, the network output for a given test sample  $\mathbf{x}_{test} = [\text{Re}(\hat{\mathbf{C}}_{test}), \text{Im}(\hat{\mathbf{C}}_{test})]$  is also a random variable. If each realization of  $\mathbf{w}$  yields a different output for the same input  $\mathbf{x}_{test}$ , the model is considered uncertain about the output. MUMI [29] quantifies the amount of information that we would obtain had we received the true label (acoustic source range)  $d_{test}$  for the corresponding  $\mathbf{x}_{test}$ . This is represented in terms of the mutual information [39]  $I(d_{test}; \mathbf{w} | \mathcal{D}_{tr}, \mathbf{x}_{test})$ , where the conditioning over  $\mathcal{D}_{tr}$  is because we have used the training data to obtain  $\mathbf{w}$ . Expanding this mutual information yields

$$\begin{aligned} I(d_{test}; \mathbf{w} | \mathcal{D}_{tr}, \mathbf{x}_{test}) &= H(p(d_{test} | \mathcal{D}_{tr}, \mathbf{x}_{test})) \\ &\quad - \mathbb{E}_{p(\mathbf{w} | \mathcal{D}_{tr})} [H(p(d_{test} | \mathcal{D}_{tr}, \mathbf{w}, \mathbf{x}_{test}))], \end{aligned} \quad (6)$$

where for a given function  $h$ ,  $\mathbb{E}_{p(\mathbf{w} | \mathcal{D}_{tr})}[h(\mathbf{w})]$  denotes the expectation of the random variable  $h(\mathbf{w})$  when  $\mathbf{w}$  is distributed according to the probability density function  $p(\mathbf{w} | \mathcal{D}_{tr})$ . Although computing  $\mathbb{E}_{p(\mathbf{w} | \mathcal{D}_{tr})}[h(\mathbf{w})]$  is intractable in general, a

dropout approximating distribution  $q_\theta(\mathbf{w}|\mathcal{D}_{tr})$  can efficiently approximate  $p(\mathbf{w}|\mathcal{D}_{tr})$  [29], where  $\theta$  represents the parameters of a dropout neural network and each realization of the dropout mask corresponds to a sampling from  $q_\theta(\mathbf{w}|\mathcal{D}_{tr})$  that yields a different weight vector  $\mathbf{w}_j$ . Accordingly, the label likelihood  $p(d_{\text{test}}|\mathcal{D}_{tr}, \mathbf{x}_{\text{test}})$  in (6) can be computed by marginalization over  $\mathbf{w}$  and a Monte-Carlo approximation as

$$\begin{aligned} p(d_{\text{test}}|\mathcal{D}_{tr}, \mathbf{x}_{\text{test}}) &\approx \int p(d_{\text{test}}|\mathbf{w}, \mathcal{D}_{tr}, \mathbf{x}_{\text{test}})q_\theta(\mathbf{w}|\mathcal{D}_{tr})d\mathbf{w} \\ &\triangleq \frac{1}{J} \sum_{j=1}^J \hat{p}(\hat{y}_j|\mathbf{w}_j, \mathcal{D}_{tr}, \mathbf{x}_{\text{test}}) \\ &= \frac{1}{J} \sum_{j=1}^J \hat{p}(\hat{y}_j|\mathbf{w}_j, \mathbf{x}_{\text{test}}), \end{aligned} \quad (7)$$

where  $\mathbf{w}_j \sim q_\theta(\mathbf{w}|\mathcal{D}_{tr}), j = 1, \dots, J$  are weights sampled from the dropout network with  $J$  different dropout realizations,  $\hat{y}_j$  is the network output corresponding to the weight vector  $\mathbf{w}_j$ , and  $\hat{p}$  is the empirical likelihood of the model output. Since the training data has been used to obtain  $\mathbf{w}$ , there is a Markov chain  $\mathcal{D}_{tr} - \mathbf{w} - \hat{y}_j$ , hence,  $\hat{p}(\hat{y}_j|\mathcal{D}_{tr}, \mathbf{w}_j, \mathbf{x}_{\text{test}}) = \hat{p}(\hat{y}_j|\mathbf{w}_j, \mathbf{x}_{\text{test}})$ . Similarly,  $p(d_{\text{test}}|\mathbf{w}, \mathcal{D}_{tr}, \mathbf{x}_{\text{test}})$  can be approximated with  $\hat{p}(\hat{y}_j|\mathbf{w}_j, \mathbf{x}_{\text{test}})$ , which results in

$$\begin{aligned} \mathbb{E}_{p(\mathbf{w}|\mathcal{D}_{tr})} [H(p(d_{\text{test}}|\mathcal{D}_{tr}, \mathbf{w}, \mathbf{x}_{\text{test}}))] \\ \approx \frac{1}{J} \sum_{j=1}^J H(\hat{p}(\hat{y}_j|\mathbf{w}_j, \mathbf{x}_{\text{test}})). \end{aligned} \quad (8)$$

Substituting (7) and (8) in (6) yields

$$\begin{aligned} I(d_{\text{test}}; \mathbf{w}|\mathcal{D}_{tr}, \mathbf{x}_{\text{test}}) &\approx H\left(\frac{1}{J} \sum_{j=1}^J \hat{p}(\hat{y}_j|\mathbf{w}_j, \mathbf{x}_{\text{test}})\right) \\ &\quad - \frac{1}{J} \sum_{j=1}^J H(\hat{p}(\hat{y}_j|\mathbf{w}_j, \mathbf{x}_{\text{test}})). \end{aligned}$$

Note that MUMI can be used for both classification and regression networks. While in a classification network the output vector  $\hat{\mathbf{y}}_j$  is effectively  $\hat{p}(\hat{y}_j|\mathbf{w}_j, \mathbf{x}_{\text{test}})$ , to obtain the empirical likelihood  $\hat{p}(\hat{y}_j|\mathbf{w}_j, \mathbf{x}_{\text{test}})$  in a regression model, we quantize and one-hot encode the output of the regression network, leading to  $H(\hat{p}(\hat{y}_j|\mathbf{w}_j, \mathbf{x}_{\text{test}})) = 0$ . Thus, the MUMI reduces to

$$I(d_{\text{test}}; \mathbf{w}|\mathcal{D}_{tr}, \mathbf{x}_{\text{test}}) \approx H\left(\frac{1}{J} \sum_{j=1}^J \hat{p}(\hat{y}_j|\mathbf{w}_j, \mathbf{x}_{\text{test}})\right). \quad (9)$$

Figure 3 shows that when presented with samples from a mismatched environment, a pre-trained regression model will have a higher MUMI. This shows that the average MUMI increases with the increase in depth mismatch or SSP mismatch. This behavior is similar to the increased MUMI of DL models during adversarial attacks discussed in [29]. Also, MUMI is seen to be a monotonically increasing function of the mismatch amount.

## B. Peakwise Uncertainty (PU)

While MUMI is theoretically motivated, the MC-dropout requires  $J$  realizations of the dropout layers to obtain  $\{\hat{p}(\hat{y}_j|\mathbf{w}_j, \mathbf{x}_{\text{test}})\}_{j=1}^J$  which is not feasible for underwater low-power applications. Here, we propose a simpler method to assess uncertainty in the classification approach tailored to the localization problem. This method counts the number of significant peaks in the output PMF, and asserts that the model is certain about the corresponding result if there is only one significant peak. Following this approach, we define a significant peak as a peak that is either the only peak or is larger than the next-largest peak by a factor  $Q$ . The hyperparameter  $Q$  should be selected to draw a trade-off between the desired size of  $\mathcal{S}$  and the minimum confidence desired in pseudo labels selected. Thus

$$PU(\mathbf{x}) = \begin{cases} 0 & \text{if } \hat{\mathbf{y}} \text{ has only 1 significant peak} \\ 1 & \text{if } \hat{\mathbf{y}} \text{ has more than 1 significant peak} \end{cases} \quad (10)$$

where  $\hat{\mathbf{y}}$  is the classification network output probability vector. Throughout the paper, we use  $Q = 10$ . The average PU indicates the percentage of samples about which the model is uncertain. Figure 4 shows that the average PU increases as the amount of mismatch increases.

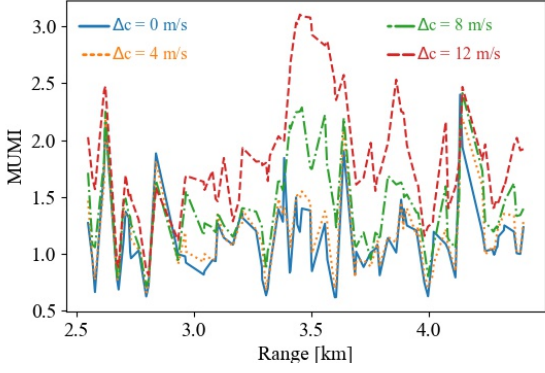
As illustrated in the example in Fig. 5, the largest peak in the output of the pre-trained model is not necessarily aligned with the true label. The JSEA algorithm introduced in the next section, determines which peak to select.

## IV. TEST TIME ADAPTATION

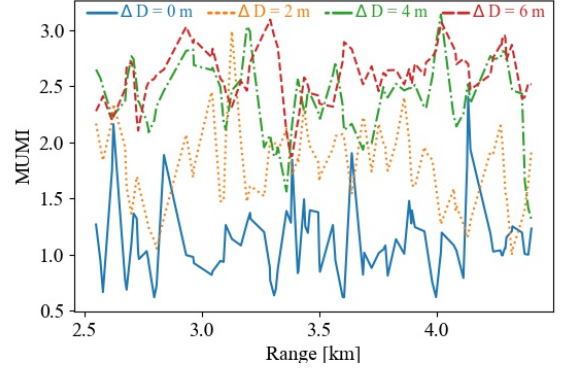
Our proposed TTA method, similar to SHOT [11], assumes that the DL-based model consists of a domain-dependent feature extractor and a domain-independent classifier (hypothesis). During inference, while freezing the classifier, SHOT fine-tunes the feature extractor to produce confident outputs and prevents it from a degenerate solution using an information maximization loss [11] that promotes diverse output labels. Although this procedure works well for one-hot coded labels, it must be adjusted for ranging tasks, where labels are not equidistant.

### A. Environmental Adaptation Using SHOT

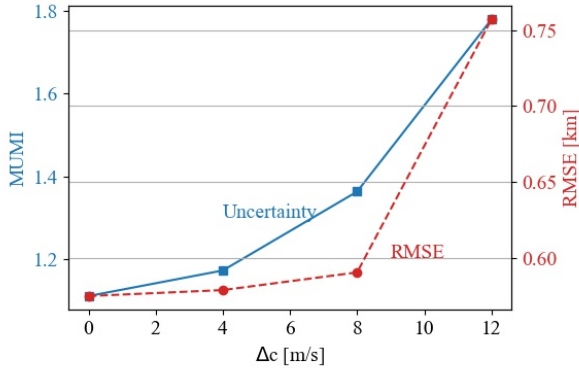
When presented with data from an environment that is markedly different from the one on which it was trained, the network makes *uncertain* predictions, i.e., it is likely to be more confused between different classes, which leads to inaccurate predictions. During inference, the absence of test labels makes fully-supervised adaptation impossible. Nevertheless, encouraging the model to more confidently preserve its predictions on samples that match to the training data, helps it overcome slight mismatches. To this end, we select a self-supervising subset  $\mathcal{S}$  of the samples and use the pre-trained network's output on these samples as their pseudo-labels, for which we use a loss term  $\text{CE}(\mathbf{y}_i^{\text{pseudo}}, \hat{\mathbf{y}}_i)$ . Here,  $\mathbf{y}_i^{\text{pseudo}}$  is the softened label based on the output of the pre-trained classifier. However, this loss and approach can create a degenerate situation where the network only predicts classes that exist



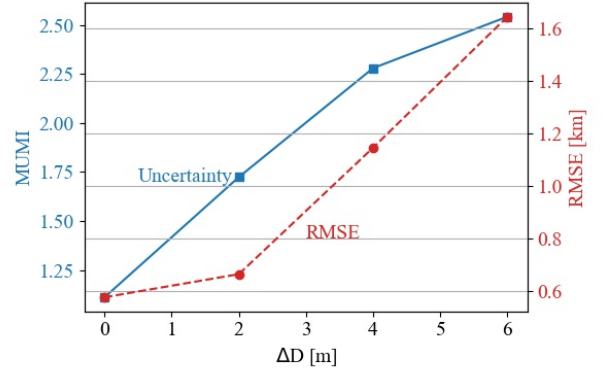
(a) Uncertainty under SSP mismatch.



(b) Uncertainty under depth mismatch.



(c) Average uncertainty under SSP mismatch.



(d) Average uncertainty under depth mismatch.

Fig. 3: MUMI uncertainty of a regression dropout network reveals the mismatch between the training and test environments. These are using the SWellEx-96-inspired synthetic data, consisting of a shallow source with a monotone signal at  $f = 109$  Hz and all of the results are averaged over 100 independent realizations of an additive white Gaussian noise (AWGN) channel. Top row shows that the uncertainty is different for each sample and the bottom row shows that, on average, both the uncertainty and the root-mean-squared-error (RMSE) increase with the amount of mismatch.

in  $\mathcal{S}$  [11]. Adding a regularizing loss term to maximize the entropy of the outputs average  $\bar{\mathbf{y}} = \frac{1}{N_{test}} \sum_{i=1}^{N_{test}} \hat{\mathbf{y}}_i$  can prevent this situation.

At the test time, we freeze the pre-trained classifier as depicted in Fig. 1, which predicts the label  $\hat{\mathbf{y}}_i = [\hat{y}_{i1}, \hat{y}_{i2}, \dots, \hat{y}_{iM}]$  by applying the Softmax() operation to  $\omega_k^T \phi_i$ , i.e.,

$$\hat{y}_{ik} = \frac{\exp(\omega_k^T \phi_i)}{\sum_{k=1}^M \exp(\omega_k^T \phi_i)}, \quad (11)$$

and  $\omega_k$  is the classification weight vector corresponding to the  $k$ -th class. Note that if the feature vector  $\phi_i$  is highly aligned with  $\omega_{k_0}$  for only one  $k_0$ , then the network predicts a unimodal soft label  $\hat{\mathbf{y}}_i$ , as opposed to situations where the network generates a multimodal output and is not certain about the predicted label. Inspired by this observation, we construct the self-supervising subset  $\mathcal{S}$  according to

$$\mathcal{S} = \{i : 1 \leq i \leq N_{test} \text{ s.t. } PU(\mathbf{x}_i) = 0\}. \quad (12)$$

To perform the adaptation, we minimize the SHOT loss

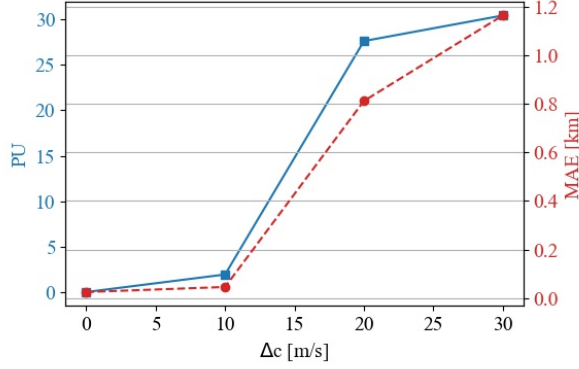
defined by

$$\mathcal{L}_{SHOT} = -H(\bar{\mathbf{y}}) + \frac{\beta}{|\mathcal{S}|} \sum_{i \in \mathcal{S}} \text{CE}(\mathbf{y}_i^{\text{pseudo}}, \hat{\mathbf{y}}_i), \quad (13)$$

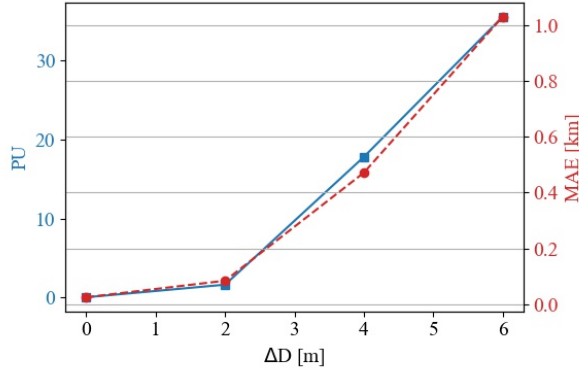
where,  $\beta$  is a positive hyperparameter. We then employ the Adam optimizer [40] to minimize  $\mathcal{L}_{SHOT}$  with a step size of  $\mu_{SHOT}$ . The cross-entropy term encourages the network to remain certain about its existing confident predictions, while increasing  $H(\bar{\mathbf{y}})$  prevents it from assigning all inputs to the same output by encouraging diverse outputs [11]. Although effective at rectifying errors due to small mismatches, SHOT does not directly enhance the estimates for samples in  $\mathcal{S}^c$  and does not focus on removing the model's confusions. To alleviate this, we now introduce another adaptation mechanism that explicitly selects pseudo-labels for the samples in  $\mathcal{S}^c$ .

### B. Joint Source-Environment Adaptation (JSEA)

While TTA methods in the machine learning literature focus on *domain* adaptation, they do not consider or distinguish the *source* that generates data and the *environment* where data



(a) Uncertainty under SSP mismatch.



(b) Uncertainty under depth mismatch.

Fig. 4: Variation of the peakwise uncertainty with the amount of environmental mismatch in (a) depth and (b) SSP.

is generated. In UWA, however, there is a clear distinction between these two factors. To improve the generalization performance of data-driven methods in UWA signal processing, a necessary step is normalization with respect to the source, which effectively yields source-invariant features and better generalization across different sources. Accordingly, array-based localization usually involves normalization by the total received signal power at the array elements. According to Fig. 6, the array SNR at the given frequency can provide a range estimate that (i) is coarse, due to the local fluctuations in the signal power level, but (ii) is robust because the general trend is that higher SNR is associated with a closer source, regardless of the environment. To exploit the distinction between the source and the environment, we implicitly estimate the test source power from a limited set of reliable samples (samples with a unimodal output PMF). We then develop a signal strength-based approach to estimate the range of more difficult samples (samples with a multimodal output PMF). This results in combining the DL-based and signal strength-based approaches in a Bayesian manner to fully use the information in an efficient manner.

The method is detailed as follows. Given that  $\mathbf{C} = \psi \tilde{\mathbf{C}}$ , where  $\psi = \sum_{l=1}^L |r_l^{(p)}(f)|^2$  (which is an accurate definition of received signal power for  $P = 1$  snapshot case and an approximate estimate for  $P > 1$ ), and assuming that  $\psi$  and  $\tilde{\mathbf{C}}$

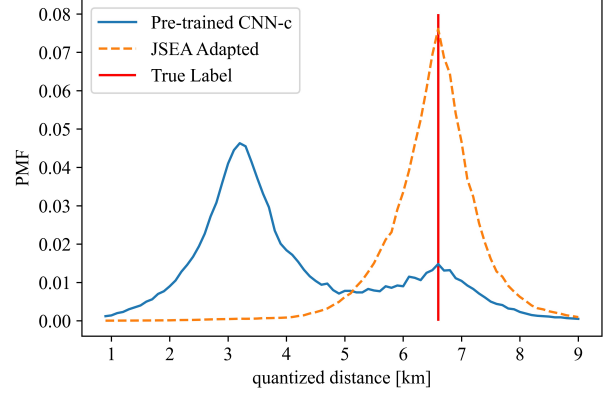


Fig. 5: An example of a predicted label in a test environment with a different SSP than the training environment. The quantization bins are 100 m wide. Observe that the pre-trained model prediction (the label with maximum probability) is far from the ground-truth. However, there is another peak in the output closer to the ground-truth.

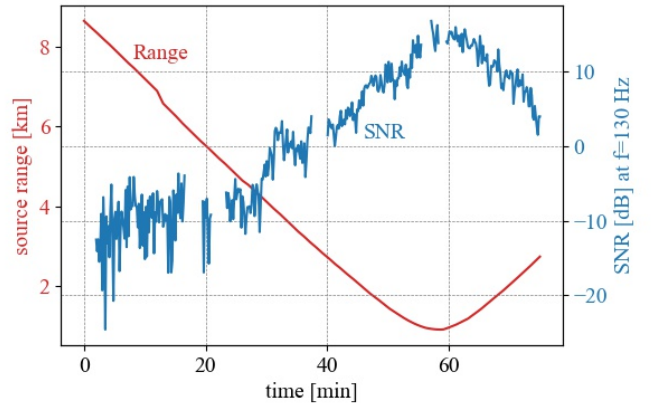


Fig. 6: The received SNR (blue) on the vertical linear array at frequency  $f = 130$  Hz, emitted from the deep source in the event S5 of the SWellEx-96 experiment [41], and source range from the receiver (red). The gaps in the SNR plot indicate some time intervals during which transmission was stopped and the array recorded only the ambient noise. These were used for the SNR calculation.

are independent, by Bayes' theorem

$$\begin{aligned} p(d|\mathbf{C}) &= p(d|\tilde{\mathbf{C}}, \psi) = \frac{p(\tilde{\mathbf{C}}, \psi|d)p(d)}{p(\tilde{\mathbf{C}})p(\psi)} \\ &= \frac{p(\tilde{\mathbf{C}}|\psi, d)p(\psi|d)p(d)}{p(\tilde{\mathbf{C}})p(\psi)} = \frac{p(d|\tilde{\mathbf{C}})p(d|\psi)}{p(d)}. \end{aligned} \quad (14)$$

As a result, if  $d$  is uniformly distributed over the parameter space of interest, we have  $p(d|\mathbf{C}) \propto p(d|\tilde{\mathbf{C}})p(d|\psi)$ . The received signal power  $\psi$  depends on the source power that can be estimated from  $\mathcal{S}$  in (12). Note that both  $p(d|\tilde{\mathbf{C}})$  and  $p(d|\psi)$  can be used for localization:  $p(d|\tilde{\mathbf{C}})$  provides a finer estimate based on the normalized SCM (and typically more

sensitive to mismatches), while  $p(d|\psi)$  provides a coarser estimate based on the received signal power that is more robust to environmental mismatches. Since both estimates use different and independent pieces of information, by exploiting both terms we can significantly improve the performance of localization algorithms in the presence of mismatches.

For each sample in  $\mathcal{D}_{test}$ , the pre-trained classification model generates  $\hat{\mathbf{y}}_i = \hat{p}(d|\mathbf{C})$ . After partitioning the samples into  $\mathcal{S}$  and  $\mathcal{S}^c$  based on their peakwise uncertainty, the final range  $\hat{d}_i$  estimate for  $\mathbf{x}_i \in \mathcal{S}$  is the distance corresponding to the only peak of  $\hat{\mathbf{y}}_i$ . For  $\mathbf{x}_i \in \mathcal{S}^c$ , let  $\mathcal{P}(\hat{\mathbf{y}}_i)$  be the set of distances corresponding to all significant peak locations of  $\hat{\mathbf{y}}_i$ . The goal is to determine a member of  $\mathcal{P}(\hat{\mathbf{y}}_i)$  as the pseudo-label for  $\mathbf{x}_i$  by exploiting

$$\hat{d}_i = \arg \max_{d \in \mathcal{P}(\hat{\mathbf{y}}_i)} p(d|\psi = \psi_i). \quad (15)$$

In a homogeneous boundary-less acoustic medium, the received power (on a single hydrophone) from a point source at distance  $d$  is proportional to  $1/d$ . In ocean waveguides, however, the received power fluctuates around a decreasing function  $\psi_0(d)$ ; the fluctuations are affected by the ocean variability and ambient noise as well, leading to the low resolution of the estimates based on  $p(d|\psi)$ . Assuming that  $\psi(d)$  is normally distributed with the mean  $\psi_0(d)$  and considering a non-informative prior distribution on  $\psi$ , (15) reduces to

$$\hat{d}_i = \arg \min_{d \in \mathcal{P}(\hat{\mathbf{y}}_i)} (\psi_i - \psi_0(d))^2. \quad (16)$$

Since  $\psi_0$  is unknown, we approximate  $\psi_0(d)$  for each  $d \in \mathcal{P}(\hat{\mathbf{y}}_i)$  using the samples in  $\mathcal{S}$  with [6]  $\hat{\psi}_0(d) = \frac{1}{|\mathcal{S}_\delta(d)|} \sum_{j \in \mathcal{S}_\delta(d)} \psi_j$ , where  $\mathcal{S}_\delta(d) = \{j \in \mathcal{S}; |d - \hat{d}_j| \leq \delta\}$ , and  $\psi_j$  is the received power of the  $j$ -th sample. Therefore,

$$\hat{d}_i = \arg \min_{d \in \mathcal{P}(\hat{\mathbf{y}}_i)} \left( \psi_i - \frac{1}{|\mathcal{S}_\delta(d)|} \sum_{j \in \mathcal{S}_\delta(d)} \psi_j \right)^2. \quad (17)$$

By defining the pseudo-labels for  $\mathbf{x}_i$  as  $\mathbf{y}_i^{\text{pseudo}} \triangleq \eta(\hat{d}_i)$ , we have achieved the range estimates for all given test samples. If the model is to be used for another source in the same environment, one should also adapt the feature extractor by minimizing the JSEA loss defined by  $\mathcal{L}_{\text{JSEA}} = \sum_{i=1}^{N_{test}} \text{CE}(\mathbf{y}_i^{\text{pseudo}}, \hat{\mathbf{y}}_i)$ .

## V. EMPIRICAL EVALUATION

### A. Synthetic data

We first consider data generated using KRAKEN [42], where the environmental parameters are set according to the SWellEx-96 [4], [37] experiment. As depicted in Fig. 7, the training data consist of source ranges between 0.85 km and 9.05 km with 10 m increments (thus, 821 distinct samples), and a 21-element vertical linear array placed at depths from 94.125 m to 212.25 m to mimic the SWellEx-96 data. The source depth is assumed to be 9 m and transmits a monotone signal at a frequency of  $f = 109$  Hz. We consider a flat bathymetry at depth 216.5 m in our simulations and used the average SSP from the SWellEx-96 measurements. The bottom constitutes of 3 layers whose depths, densities, and attenuation match the SWellEx-96 environment.

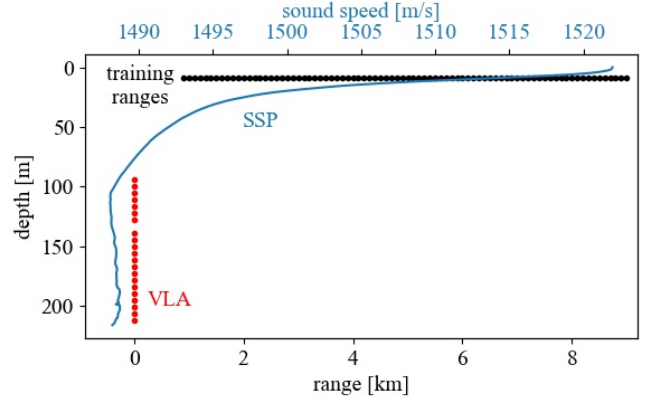


Fig. 7: KRAKEN environment based on the SWellEx-96 experiment. The receiver array is a 21-element array depicted in red. The uniformly sampled source ranges that are used for training are shown with black dots. Also the SSP, which is the average SSP from the SWellEx-96 experiment, is shown with the blue graph.

To generate a test environment that has a sound-speed  $c(z)$  at depth  $z$ , which is mismatched with that of the training environment,  $c_0(z)$ , we perturb  $c_0(z)$  using a constant gradient difference of  $\Delta c$  (m/s)/m, represented as  $c(z) = c_0(z) + \frac{\Delta c}{216.5}(z - 216.5)$ , where  $0 \leq z \leq 216.5$  m. We generate data for 500 random source ranges between  $D_{\min} = 900$  m and  $D_{\max} = 9$  km, and divide the region into 100 m-long intervals, each represented by its mid point. Consequently, the labels and classifier outputs are 82-dimensional (i.e.,  $M = 82$ ). In addition, to emulate the real ocean ambient noise during test time, we add a randomly selected noise segment  $w$  from the KAM11 experiment [43] (scaled to have a desired signal-to-noise ratio in the data) to the generated signal for each hydrophone. Since the proposed method takes a batch of test data, we use the average array SNR of the batch, defined as

$$\text{SNR [dB]} = 10 \log_{10} \frac{\sum_{i=1}^{N_{test}} \sum_{l=1}^L |r_{i,l}|^2}{N_{test} L \psi_w},$$

where  $|r_{i,l}|^2$  is the received signal power at the  $l$ -th hydrophone of the  $i$ -th sample and  $\psi_w$  is the noise power spectral density at the frequency  $f = 109$  Hz.

We evaluate models using MAE and probability of credible localization (PCL) [16] defined as

$$\text{PCL}(\zeta) = \frac{100}{N_{test}} \sum_{i=1}^{N_{test}} \mathbf{1}_{|d_i - \hat{d}_i| \leq \zeta d_i},$$

$$\text{MAE} = \frac{1}{N_{test}} \sum_{i=1}^{N_{test}} |d_i - \hat{d}_i|,$$

where  $d_i$  and  $\hat{d}_i$  are respectively the true and estimated distances of the  $i$ -th sample. Probability of credible localization can be interpreted as the probability that the range estimate lies within a certain percentage bound of the true range, defined here as  $\zeta = 10\%$ .

The methods evaluated include:

- O-MFP (Oracle-MFP): The MFP approach tuned to the test environment. This method is presented just for reference and is expected to outperform all other methods because it has access to the test environment parameters.
- M-MFP (mismatched MFP): The MFP approach tuned to the training environment. This method, in contrast with data-driven methods, has access to the training data.
- CNN-c: A CNN-based model for classification.
- SHOT: The CNN-c equipped with the adaptation mechanism in (13), with  $\mu_{\text{SHOT}} = 5 \times 10^{-6}$  and  $\beta = 1$ .
- JSEA-c: The CNN-c equipped with the pseudo-label estimator in (17), where  $\delta = 500$  m.
- CNN-r: A CNN-based model for regression.
- JSEA-r: The CNN-r followed by an MC-dropout mechanism to generate output PMFs and equipped with the pseudo-label estimator in (17), where  $\delta = 500$  m.

To select the label smoothing hyperparameter  $\sigma$ , we compared the performance of the trained model on the validation data for different values of  $\sigma$  and found that  $\sigma = 2$  works well. We also use a learning rate of  $10^{-4}$  and a batch size of 128 for the Adam optimizer. We randomly split the set of uniformly sampled ranges into 82% training and 18% validation sets. To prevent over-fitting and converge better to the minimum, we adopt a decreasing learning rate - we multiply the learning rate by 0.1 whenever there is no reduction in the validation error after 75 iterations, and we stop training if there is no reduction in the validation error after 125 iterations [3]. To enhance robustness against noise, after training the network with clean training data, we continue training with noisy data, where the inputs are contaminated by white Gaussian noise with an SNR in  $\{2, 4, 6, 8, 10, 12, 14, 16\}$  dB. The test results are averaged over 100 noise realizations.

Figure 8 shows the superiority of the JSEA-c and CNN-c methods over M-MFP when the training and testing environments have a depth mismatch of  $\Delta D = 4$  m (i.e., the ocean depth in the test environment is 220.5 m), and there is a mismatch in the noise statistics of the test data compared to the training data as well. The proposed JSEA-c outperforms other methods including SHOT, however, its improvement highly depends on the success of the pre-trained model in generating enough certain labels. Although, JSEA-r can successfully improve the regression results as seen in Fig. 8, we will not include the regression models in the following experiments due to their inferior performance. In this scenario, the M-MFP shows inferior performance with respect to classification methods, in the presence of depth mismatch.

Figure 9 shows the performance comparison of the methods with variation in the degree of SSP mismatch. In the current scenario, mismatch in SSP gradient is assessed, by varying the gradient difference  $\Delta c$  between training and test data. As seen in Fig. 9, the M-MFP outperforms the DL models; however, it benefits from using training data during inference, which is not available to the other methods. While SHOT can improve the CNN-c results, JSEA-c has the best performance among the DL methods.

Next we consider the depth mismatch and evaluate the performance of the algorithms for  $\Delta D \in \{0, 2, 4, 6\}$  m/s.

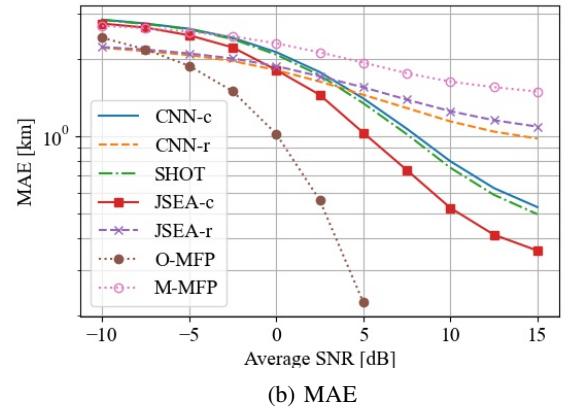
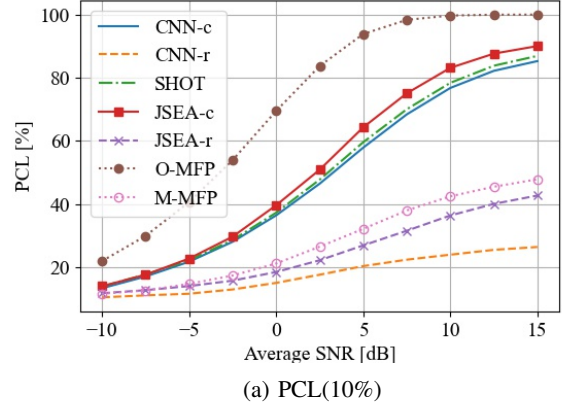


Fig. 8: Performance versus SNR using noise data from KAM11 experiment and with  $\Delta D = 4$  m for the shallow source with the monotone signal at  $f = 109$  Hz, evaluated with metrics: (a) PCL and (b) MAE. While the O-MFP provides a performance bound as it has access to training data generated in an environment matched to the test environment, the M-MFP shows the performance degradation of the MFP method when provided with the mismatched data.

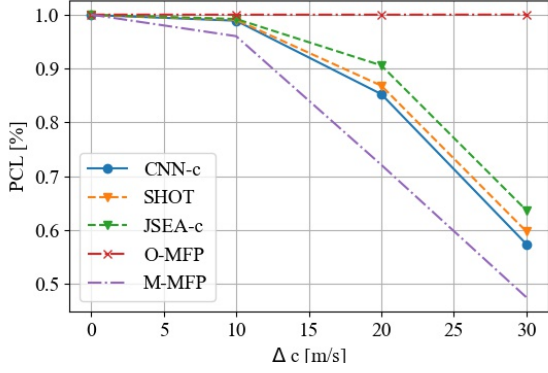
As seen in Fig. 10, when the test and training environments match (i.e.,  $\Delta D = 0$ ), the MFP (in this case, the M-MFP is not mismatched, hence it is the same as O-MFP) performs the best. However, depth mismatches lead to the M-MFP's performance deterioration, whereas the performance of the CNN-based methods is more robust to this mismatch. Thus, using CNN methods can impart some robustness to localization performance under depth mismatch.

Overall, we observe that using TTA can enhance the performance of the CNN-based approach by allowing better adaptation to the test environment and introducing more robustness to mismatch. This is demonstrated by the improvement in SHOT and JSEA in comparison to CNN. Using the received signal power information further improves the performance, as seen in the improvement in JSEA as compared to SHOT.

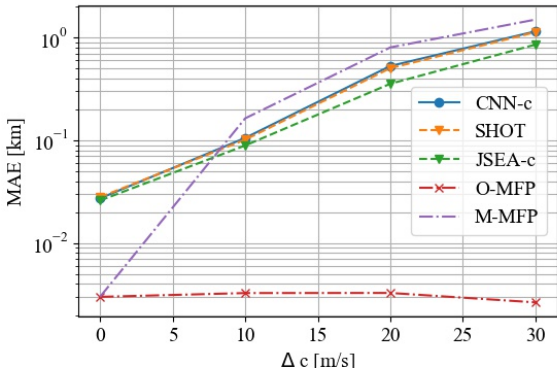
### B. SWellEx-96 Data

We use data from the event S5 of the public dataset SWellEx-96 experiment [41], [44], [45]. In this event, two





(a) PCL(10%) under mismatch in SSP.



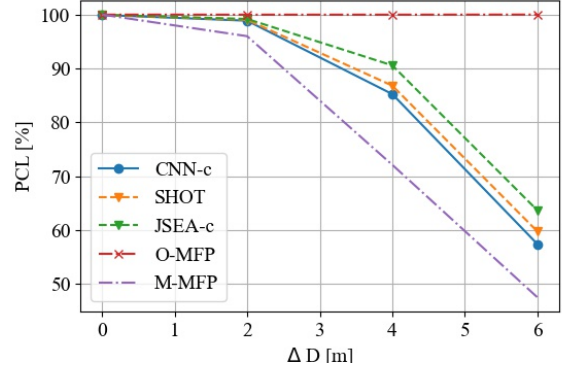
(b) MAE under mismatch in SSP.

Fig. 9: Performance against variation in SSP mismatch at an SNR of 15 dB.

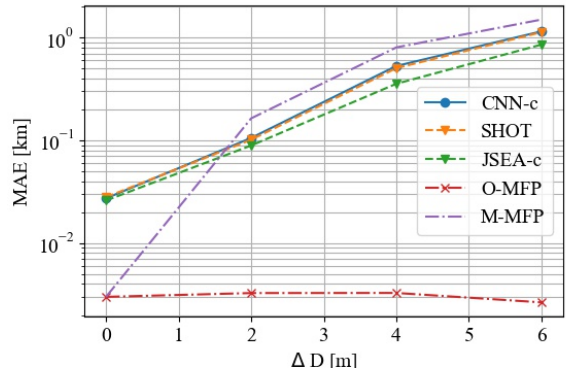
sources, a shallow source at a depth of 9 m and a deep source at a depth of 54 m, were towed by a ship moving in a straight line as shown in Fig. 11. The whole event took 75 minutes, during which each source transmitted a set of frequencies with a specific power level, recorded by several arrays at the sampling frequency of  $F_s = 1500$  Hz. We use the recordings from the 21-element ( $L = 21$ ) vertical line array (VLA) and provide the results for the shallow source.

To obtain the Fourier transform and the corresponding SCM  $\mathbf{C}$  used for localization, we use a 3-second-long signal divided into  $P = 5$  segments, each of length 1 second and a 50% overlap, tapered by a Kaiser window with  $\beta = 9.24$ . We obtain the true source range by linear interpolation between the GPS recordings provided.

Figure 12 shows the ranging results of M-MFP, CNN-c, and JSEA-c on the real-world narrow-band data at frequency  $f = 109$  Hz. The results in Fig. 12a suggest that M-MFP performs poorly in this scenario, as it leans towards overestimating the ranges for the samples around  $t = 60$  min which are closest to the VLA and have a relatively higher SNR. This problem is absent in the CNN-c approach as observed in Fig. 12b. Nevertheless, both M-MFP and CNN-c tend to deviate significantly from the true ranges in the low SNR regions, i.e., larger source ranges ( $t \leq 40$  min). Whereas this problem is still present in JSEA-c, it is considerably less



(a) PCL(10%) under mismatch in SSP.



(b) MAE under mismatch in SSP.

Fig. 10: Performance against variation in magnitude of depth mismatch at an SNR of 15 dB.

TABLE I: Localization performance for SWellEx-96 data.

	M-MFP	CNN-c	JSEA-c
MAE [km]	2.387	1.746	1.430
PCL (20%)	31.78	38.89	42.67

severe, yielding an overall better MAE and PCL, as shown in Table I.

To understand the effect of the JSEA-c approach on reducing the error, we show the partitioning of the samples into certain and uncertain sets based on the PU scores, in Fig. 4. This figure denotes that most of the uncertain samples are in the low SNR region, where the M-MFP and CNN-c fail. This means that the JSEA-c approach relies on the certain samples (mainly the correctly estimated samples which tend to be from the high SNR region) to rectify the incorrect outputs of the CNN-c. This might also be, in part, due to the fact the samples around  $t = 60$  min are not only higher in SNR, but also their environment is matched the most to the training environment, as the depth we use for training environment is 216.5 m, which is the depth at the VLA location.

## VI. CONCLUSION

We showed that an appropriate model uncertainty such as MUMI has the potential to reveal the mismatch between the training and test environments. However, since regression

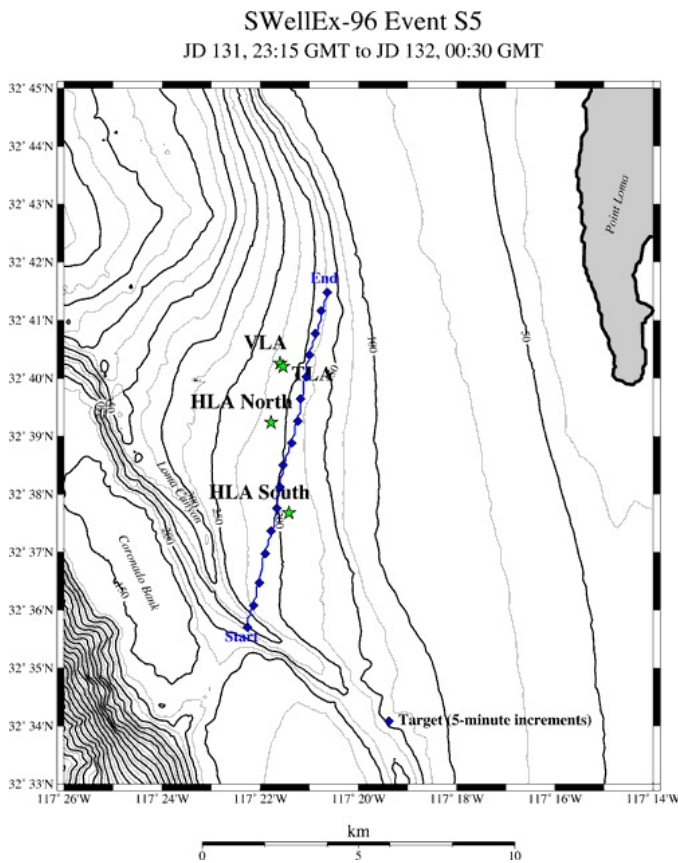


Fig. 11: The ship track for the SWellEx-96 S5 event [41]. We aim to estimate the distance of the ship to the VLA receiver.

models equipped with MUMI are computationally complex, we resort to a classification paradigm, where we used a special label softening to tailor the method to localization. By using classification for localization, the model outputs reveal the peakwise uncertainty, which we then use to enhance the localization based on the source power.

We showed that while SHOT can slightly improve the performance by encouraging the network to make its predictions less uncertain on the samples that are similar to the training set, JSEA can further improve the UWA localization performance on the samples that suffer more from the environmental mismatch. To be successful, the proposed JSEA method requires a pre-trained model that can correctly classify part of the test data and do so with certainty.

This paper shows that by suitable domain adaptation, one can enhance localization robustness in data-driven methods. With more prior knowledge about domain shifts between the training and testing environments and source location distribution, one may be able to improve the performance by using more effective methods for selecting  $S$  even without access to training data. However, the performance improvement will be limited in the absence of such knowledge. Future potential directions on this front include investigating other TTA methods currently used for other machine learning problems and developing other methods uncertainty quantification in the stated UWA problem.

## REFERENCES

- [1] H. Niu, E. Reeves, and P. Gerstoft, "Source localization in an ocean waveguide using supervised machine learning," *J. Acoust. Soc. Amer.*, vol. 142, no. 3, pp. 1176–1188, 2017.
- [2] J. Yangzhou, Z. Ma, and X. Huang, "A deep neural network approach to acoustic source localization in a shallow water tank experiment," *J. Acoust. Soc. Amer.*, vol. 146, no. 6, pp. 4802–4811, 2019.
- [3] R. Chen and H. Schmidt, "Model-based convolutional neural network approach to underwater source-range estimation," *J. Acoust. Soc. Amer.*, vol. 149, no. 1, pp. 405–420, 2021.
- [4] Y. Wang and H. Peng, "Underwater acoustic source localization using generalized regression neural network," *J. Acoust. Soc. Amer.*, vol. 143, no. 4, pp. 2321–2331, 2018.
- [5] Y. Liu, H. Niu, Z. Li, and D. Zhai, "Unsupervised domain adaptation for source localization using ships of opportunity with a deep vertical line array," *IEEE J. Ocean. Eng.*, 2023.
- [6] D. Kari and A. C. Singer, "Joint source-environment adaptation for deep learning-based underwater acoustic source ranging," in *Asilomar Conf. Signals, Syst., Comput.* IEEE, 2024.
- [7] Y. Ganin and V. Lempitsky, "Unsupervised domain adaptation by backpropagation," in *Int. Conf. Mach. Learn.* PMLR, 2015, pp. 1180–1189.
- [8] Y. Song, "Underwater acoustic sensor networks with cost efficiency for internet of underwater things," *IEEE Trans. Ind. Electron.*, vol. 68, no. 2, pp. 1707–1716, 2020.
- [9] X. Zhuo, M. Liu, Y. Wei, G. Yu, F. Qu, and R. Sun, "Auv-aided energy-efficient data collection in underwater acoustic sensor networks," *IEEE Internet Things J.*, vol. 7, no. 10, pp. 10010–10022, 2020.
- [10] W. Zhang, G. Han, X. Wang, M. Guizani, K. Fan, and L. Shu, "A node location algorithm based on node movement prediction in underwater acoustic sensor networks," *IEEE Trans. Veh. Technol.*, vol. 69, no. 3, pp. 3166–3178, 2020.
- [11] J. Liang, D. Hu, and J. Feng, "Do we really need to access the source data? source hypothesis transfer for unsupervised domain adaptation," in *Int. Conf. Mach. Learn.* PMLR, 2020, pp. 6028–6039.
- [12] A. B. Baggeroer, W. Kuperman, and H. Schmidt, "Matched field processing: Source localization in correlated noise as an optimum parameter estimation problem," *J. Acoust. Soc. Amer.*, vol. 83, no. 2, pp. 571–587, 1988.
- [13] E. J. Sullivan and D. Middleton, "Estimation and detection issues in matched-field processing," *IEEE J. Ocean. Eng.*, vol. 18, no. 3, pp. 156–167, 1993.
- [14] K. Zhang, B. Schölkopf, K. Muandet, and Z. Wang, "Domain adaptation under target and conditional shift," in *Int. Conf. Mach. Learn.* PMLR, 2013, pp. 819–827.
- [15] Y. Zhang, H. Wang, C. Li, D. Chen, and F. Meriaudeau, "Meta-learning-aided orthogonal frequency division multiplexing for underwater acoustic communications," *J. Acoust. Soc. Amer.*, vol. 149, no. 6, pp. 4596–4606, 2021.
- [16] W. Wang, H. Ni, L. Su, T. Hu, Q. Ren, P. Gerstoft, and L. Ma, "Deep transfer learning for source ranging: Deep-sea experiment results," *J. Acoust. Soc. Amer.*, vol. 146, no. 4, pp. EL317–EL322, 2019.
- [17] J. Yosinski, J. Clune, Y. Bengio, and H. Lipson, "How transferable are features in deep neural networks?" *Adv. Neural Inf. Process. Syst.*, vol. 27, 2014.
- [18] H. Yao, Y. Wang, S. Li, L. Zhang, W. Liang, J. Zou, and C. Finn, "Improving out-of-distribution robustness via selective augmentation," in *Int. Conf. Mach. Learn.* PMLR, 2022, pp. 25407–25437.
- [19] Y. Liu, H. Niu, Z. Li, and M. Wang, "Deep-learning source localization using autocorrelation functions from a single hydrophone in deep ocean," *JASA Exp. Lett.*, vol. 1, no. 3, 2021.
- [20] R. Long, J. Zhou, N. Liang, Y. Yang, and H. Shen, "Deep unsupervised adversarial domain adaptation for underwater source range estimation," *J. Acoust. Soc. Amer.*, vol. 154, no. 5, pp. 3125–3144, 2023.
- [21] Y. Zhu, F. Zhuang, J. Wang, G. Ke, J. Chen, J. Bian, H. Xiong, and Q. He, "Deep subdomain adaptation network for image classification," *IEEE Trans. Neural Netw. Learn. Syst.*, vol. 32, no. 4, pp. 1713–1722, 2020.
- [22] D. Wang, E. Shelhamer, S. Liu, B. Olshausen, and T. Darrell, "Tent: Fully test-time adaptation by entropy minimization," in *Int. Conf. Learn. Represent.*, 2021. [Online]. Available: <https://openreview.net/forum?id=uX13bZLkr3c>
- [23] J. N. Kundu, N. Venkat, R. V. Babu *et al.*, "Universal source-free domain adaptation," in *Proc. IEEE/CVF Conf. Comput. Vis. Pattern Recognit.*, 2020, pp. 4544–4553.

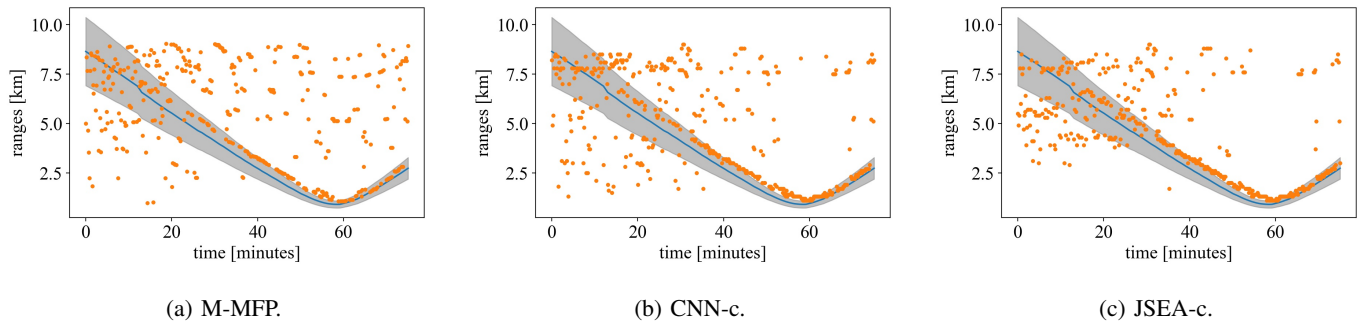


Fig. 12: Localization results for SWellEx-96 data. The blue curve indicates the ground-truth values of range at each time. The orange dots in each plot, indicate the corresponding estimated ranges. The gray cone around the blue curve indicates an interval from 0.9 to 1.1 of the true range. Observe how with JSEA, the predicted ranges are concentrated closer to the true ranges.

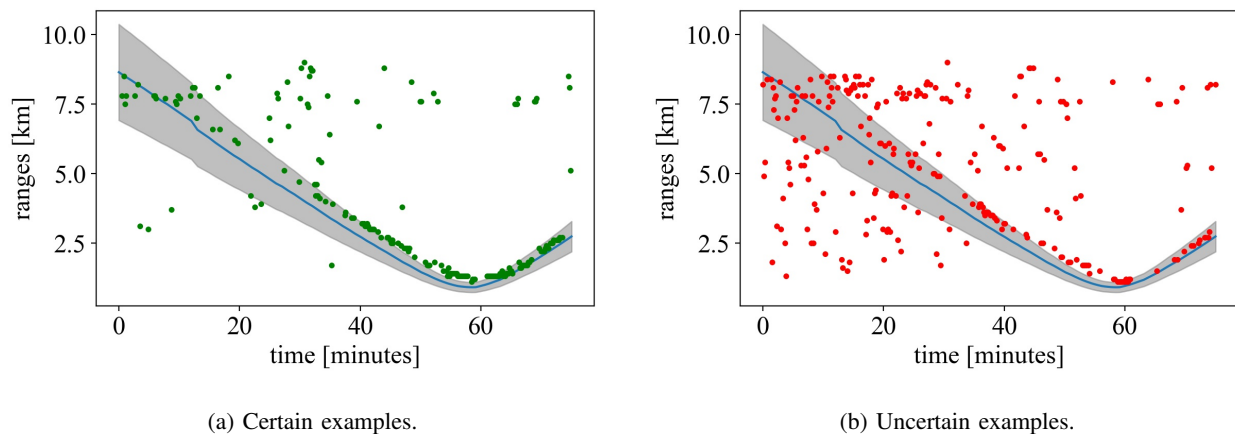


Fig. 13: Partitioning of the CNN-c predictions for SWellEx-96 data into certain and uncertain examples using PU metric. The solid blue line indicates the ground-truth. The left plot shows certain examples and the right plot shows uncertain examples.

- [24] D. Chen, D. Wang, T. Darrell, and S. Ebrahimi, "Contrastive test-time adaptation," in *Proc. IEEE/CVF Conf. Comput. Vis. Pattern Recognit.*, 2022, pp. 295–305.
- [25] H. Xia, H. Zhao, and Z. Ding, "Adaptive adversarial network for source-free domain adaptation," in *Proc. IEEE/CVF Int. Conf. Comput. Vis.*, 2021, pp. 9010–9019.
- [26] N. Ding, Y. Xu, Y. Tang, C. Xu, Y. Wang, and D. Tao, "Source-free domain adaptation via distribution estimation," in *Proc. IEEE/CVF Conf. Comput. Vis. Pattern Recognit.*, 2022, pp. 7212–7222.
- [27] J. Gawlikowski, C. R. N. Tassi, M. Ali, J. Lee, M. Humt, J. Feng, A. Kruspe, R. Triebel, P. Jung, R. Roscher *et al.*, "A survey of uncertainty in deep neural networks," *Artif. Intell. Rev.*, vol. 56, no. Suppl 1, pp. 1513–1589, 2023.
- [28] Y. Gal and Z. Ghahramani, "Dropout as a bayesian approximation: Representing model uncertainty in deep learning," in *Int. Conf. Mach. Learn.* PMLR, 2016, pp. 1050–1059.
- [29] L. Smith and Y. Gal, "Understanding measures of uncertainty for adversarial example detection," *arXiv preprint arXiv:1803.08533*, 2018.
- [30] M. Abdar, F. Pourpanah, S. Hussain, D. Rezazadegan, L. Liu, M. Ghavamzadeh, P. Fieguth, X. Cao, A. Khosravi, U. R. Acharya *et al.*, "A review of uncertainty quantification in deep learning: Techniques, applications and challenges," *Inf. Fusion*, vol. 76, pp. 243–297, 2021.
- [31] A. N. Angelopoulos and S. Bates, "A gentle introduction to conformal prediction and distribution-free uncertainty quantification," *arXiv preprint arXiv:2107.07511*, 2021.
- [32] I. D. Khurjekar and P. Gerstoft, "Uncertainty quantification for direction-of-arrival estimation with conformal prediction," *J. Acoust. Soc. Amer.*, vol. 154, no. 2, pp. 979–990, 2023.
- [33] A. Weiss, T. Arikan, H. Vishnu, G. B. Deane, A. C. Singer, and G. W. Wornell, "A semi-blind method for localization of underwater acoustic sources," *IEEE Trans. Signal Process.*, vol. 70, pp. 3090–3106, 2022.
- [34] T. Xu, Y. Hu, B. Zhang, and G. Leus, "RSS-based sensor localization in underwater acoustic sensor networks," in *2016 IEEE Int. Conf. Acoust., Speech, Signal Process. (ICASSP)*. IEEE, 2016, pp. 3906–3910.
- [35] B. Zhang, H. Wang, T. Xu, L. Zheng, and Q. Yang, "Received signal strength-based underwater acoustic localization considering stratification effect," in *OCEANS 2016 - Shanghai*, 2016, pp. 1–8.
- [36] P. Gerstoft, H. Groll, and C. F. Mecklenbräuker, "Parametric bootstrapping of array data with a generative adversarial network," in *IEEE Sens. Array Multichannel Signal Process. Workshop (SAM)*. IEEE, 2020, pp. 1–5.
- [37] K. L. Gemba, W. S. Hodgkiss, and P. Gerstoft, "Adaptive and compressive matched field processing," *J. Acoust. Soc. Amer.*, vol. 141, no. 1, pp. 92–103, 2017.
- [38] A. Weiss, T. Arikan, and G. W. Wornell, "Direct localization in underwater acoustics via convolutional neural networks: A data-driven approach," in *IEEE Int. Workshop Mach. Learn. Signal Process. (MLSP)*. IEEE, 2022, pp. 1–6.
- [39] T. M. Cover, *Elements of information theory*. John Wiley & Sons, 1999.
- [40] D. P. Kingma and J. Ba, "Adam: A method for stochastic optimization," in *ICLR (Poster)*, 2015. [Online]. Available: <http://arxiv.org/abs/1412.6980>
- [41] N. O. Booth, W. S. Hodgkiss, and D. E. Ensberg, "SWellEx-96 experiment acoustic data," 2015, UC San Diego Library Digital Collections. [Online]. Available: <https://doi.org/10.6075/J0MW2F21>
- [42] M. B. Porter, "The KRAKEN normal mode program," Naval Research Lab Washington DC, Tech. Rep., 1992.
- [43] B. Tomasi, J. Preisig, and M. Zorzi, "On the predictability of underwater

acoustic communications performance: The KAM11 data set as a case study,” in *Proc. Int. Workshop Underwater Netw.*, 2011, pp. 1–7.

- [44] P. Hursky, “Matched field processing with data-derived modes,” *J. Acoust. Soc. Amer.*, vol. 109, no. 4, pp. 1355–1366, 2001.
- [45] G. J. Orris, M. Nicholas, and J. S. Perkins, “The matched-phase coherent multi-frequency matched-field processor,” *J. Acoust. Soc. Amer.*, vol. 107, no. 5, pp. 2563–2575, 2000.



**Dariush Kari** is currently a Postdoctoral Research Associate with the Interdisciplinary Health Sciences Institute at the University of Illinois Urbana-Champaign. He received his Ph.D. in Electrical and Computer Engineering from the University of Illinois Urbana-Champaign, USA, 2024, and his M.Sc. in Electrical and Electronics Engineering from Bilkent University, Ankara, Turkey, 2017, and his B.Sc. in Electrical Engineering and in Computer Science, both from Amirkabir University of Technology, Tehran, Iran, 2014. His current research

interests include statistical signal processing, machine learning, computational acoustic sensing and imaging, photoacoustic imaging, and underwater acoustics.



**Hari Vishnu** is a Senior Research Fellow at the Acoustic Research Laboratory, National University of Singapore. His interests include machine learning for underwater applications, bio-acoustics and processing in impulsive noise. These are used in a wide range of underwater applications ranging from biodiversity or defense-related scenarios in shallow tropical waters infested with snapping shrimp noise, to polar ice sheets where glacier melt noise dominates the soundscape.

From 2019, Hari is focusing on the acoustics of melting ice, machine-learning based marine-mammal quantification, and distributed acoustic sensing. He obtained his Ph.D from Nanyang Technological University, Singapore, in Computer Engineering on underwater signal processing including robust detection and localization.

He is the Chief Editor on the IEEE OES Science outreach magazine Earthzine and serves on the IEEE Oceanic Engineering society Executive committee as Deputy Secretary. In 2019, he was awarded the IEEE OES YP-BOOST award which aims to encourage young professionals to participate in the society leadership.



**Andrew C. Singer** received the S.B., S.M., and Ph.D. degrees in electrical engineering and computer science from the Massachusetts Institute of Technology (MIT), Cambridge, MA, USA. Since 2023, he is Dean of the College of Engineering and Applied Sciences at Stony Brook University and Professor of Electrical and Computer Engineering. From 1998 to 2023 he was on the Faculty of the Department of Electrical and Computer Engineering at the University of Illinois Urbana-Champaign, where he currently is Fox Family Professor Emeritus. During

the academic year 1996, he was a Postdoctoral Research Affiliate with the Research Laboratory of Electronics, MIT. From 1996 to 1998, he was a Research Scientist with Sanders (a Lockheed Martin Company), Manchester, NH, USA. In 2000, he co-founded Intersymbol Communications, Inc., and in 2014, he co-founded OceanComm, Inc. In 2009, he was an elected Fellow of the IEEE “for contributions to signal processing techniques for digital communication,” and in 2014, he was named a Distinguished Lecturer of the IEEE Signal Processing Society.